

University of Nebraska - Lincoln

DigitalCommons@University of Nebraska - Lincoln

Food for Health Papers & Publications

Food for Health

2-3-2016

Structural and Evolutionary Analyses Show Unique Stabilization Strategies in the Type IV Pili of *Clostridium difficile*

Kurt H. Piepenbrink

Grace A. Maldarelli

Claudia F. Martinez de la Pena

Tanis C. Dingle

George L. Mulvey

See next page for additional authors

Follow this and additional works at: <https://digitalcommons.unl.edu/ffhdocs>



Part of the [Biochemical Phenomena, Metabolism, and Nutrition Commons](#), [Dietetics and Clinical Nutrition Commons](#), [Gastroenterology Commons](#), [Medical Microbiology Commons](#), and the [Medical Nutrition Commons](#)

This Article is brought to you for free and open access by the Food for Health at DigitalCommons@University of Nebraska - Lincoln. It has been accepted for inclusion in Food for Health Papers & Publications by an authorized administrator of DigitalCommons@University of Nebraska - Lincoln.

Authors

Kurt H. Piepenbrink, Grace A. Maldarelli, Claudia F. Martinez de la Pena, Tanis C. Dingle, George L. Mulvey, Amanda Lee, Erik von Rosenvinge, Glen D. Armstrong, Michael S. Donnenberg, and Eric J. Sundberg

Published in final edited form as:

Structure. 2015 February 3; 23(2): 385–396. doi:10.1016/j.str.2014.11.018.

Structural and Evolutionary Analyses Show Unique Stabilization Strategies in the Type IV Pili of *Clostridium difficile*

Kurt H. Piepenbrink¹, Grace A. Maldarelli², Claudia F. Martinez de la Peña⁴, Tanis C. Dingle⁴, George L. Mulvey⁴, Amanda Lee⁴, Erik von Rosenvinge², Glen D. Armstrong⁴, Michael S. Donnenberg^{2,3}, and Eric J. Sundberg^{1,2,3,5}

¹Institute of Human Virology, University of Maryland School of Medicine, Baltimore, MD 21201, United States of America

²Department of Medicine, University of Maryland School of Medicine, Baltimore, MD 21201, United States of America

³Department of Microbiology and Immunology, University of Maryland School of Medicine, Baltimore, MD 21201, United States of America

⁴Department of Microbiology, Immunology and Infectious Disease, University of Calgary, Calgary, Alberta, T2N 1N4, Canada

Summary

Type IV pili are produced by many pathogenic Gram-negative bacteria and are important for processes as diverse as twitching motility, biofilm formation, cellular adhesion and horizontal gene transfer. However, many Gram-positive species, including *C. difficile*, also produce Type IV pili. Here, we identify the major subunit of the Type IV pili of *C. difficile*, PilA1, and describe multiple three-dimensional structures of PilA1, demonstrating the diversity found in three strains of *C. difficile*. We also model the incorporation of both PilA1 and a minor pilin, PilJ, into the pilus fiber. Although PilA1 contains no cysteine residues, and therefore cannot form the disulfide bonds found in all Gram-negative Type IV pilins, it adopts unique strategies to achieve a typical pilin fold. The structures of PilA1 and PilJ exhibit similarities with the Type IVb pilins from Gram-negative bacteria that suggest that the Type IV pili of *C. difficile* are involved in microcolony formation.

© 2014 Elsevier Ltd. All rights reserved.

⁵Corresponding author (esundberg@ihv.umaryland.edu).

Accession Numbers

The X-ray crystal structure of PilJ is deposited in the Protein Data Bank as PDB ID 4IXJ, MBPPilA1 R202091 is 4TSM, MBP-PilA1 NAP08 is 4OGM and MBP-PilA1 CD160 is 4PE2.

Author Contributions

Structure determination and modelling were done by KHP. Genetic analysis was done by GAM and KHP. Electron microscopy was done by CFM, GLM and AL. The *pilA1* strain of *C. difficile* was engineered by TCD. Mutagenesis of *pilA1* complementation plasmids was done by CFM. Measurements of mRNA expression were made by EvR and measurements of protein expression were made by GAM. All experiments were performed under the direction of GDA, MSD or EJS.

Publisher's Disclaimer: This is a PDF file of an unedited manuscript that has been accepted for publication. As a service to our customers we are providing this early version of the manuscript. The manuscript will undergo copyediting, typesetting, and review of the resulting proof before it is published in its final citable form. Please note that during the production process errors may be discovered which could affect the content, and all legal disclaimers that apply to the journal pertain.

Introduction

Type IV pili are extracellular appendages that have been found in a variety of bacteria, both Gram-positive and Gram-negative, including *Pseudomonas aeruginosa*, *Vibrio cholerae*, *Neisseria gonorrhoeae*, *N. meningitidis*, *Salmonella enterica* serovar Typhi, *Legionella pneumophila*, enteropathogenic and enterotoxigenic *Escherichia coli*, *Streptococcus pneumoniae*, *Clostridium perfringens* and *Clostridium difficile* (Giron et al., 1991; Goulding et al., 2009; Laurenceau et al., 2013; Lee et al., 1994; Stone and Abu Kwaik, 1998; Strom and Lory, 1993; Taniguchi et al., 1995; Varga et al., 2006; Zhang et al., 2000). They are utilized in a variety of adhesive processes such as biofilm formation (O'Toole and Kolter, 1998), cellular adhesion (Rudel et al., 1995), twitching motility (Bradley, 1980; Henrichsen, 1983; Merz et al., 2000; Wall and Kaiser, 1999), and horizontal gene transfer (Seifert et al., 1988; Yoshida et al., 1999). In many cases, these properties are essential for virulence (Bieber et al., 1998; Herrington et al., 1988; Tacket et al., 1998). These fimbrial appendages are composed of many pilin proteins tightly packed in a helix to bury the hydrophobic amino-terminus of each subunit in the pilus core (Craig et al., 2004). Typically, a single pilin protein, referred to as the major pilin, has been found to predominate and the other pilin proteins included as subunits are termed minor pilins. In Type II secretion, the equivalent subunits are referred to as major and minor pseudopilins.

All Type IV pilins share certain structural features, namely a pre-pilin leader sequence, an N-terminal α -helix, which is hydrophobic for the first ~60 amino acids, and a central β -sheet. The pili they form, however, diverge based on the details of their structures, particularly in the $\alpha\beta$ loop and at the C-terminus. Nearly all pilins from Gram-negative bacteria have a disulfide bond which bounds a portion of the C-terminus referred to as the D-region. Based on the length of the pre-pilin leader peptide and sequence similarity of the N-terminal α -helix, among other factors, Type IV pili have been divided into two classes, Type IVa and Type IVb pilins. Type IVa pilins occur in a wide range of Gram-negative bacteria, while Type IVb pilins have been found only in a subset capable of colonizing the intestine and are larger, particularly in the Dregion (Craig et al., 2004).

Type IV pili are also produced by several Gram-positive species (Laurenceau et al., 2013; Melville and Craig, 2013), although they are only sparsely characterized as of yet. Genes encoding Type IV pilins and pilus biogenesis proteins have been found in all of the Clostridiales and Type IV pili have been observed in several Clostridia, including *Clostridium perfringens*, where they are required for gliding motility (Varga et al., 2006), *Ruminococcus albus* (Rakotoarivonina et al., 2002) and *Clostridium difficile* (Borriello, 1988; Goulding et al., 2009; Maldarelli et al., 2014; Piepenbrink et al., 2014). Because the *C. difficile* Type IV pili represent an opportunity to better understand both the diversity of Type IV pili and the survival strategy of *C. difficile*, we have sought to characterize the Type IV pili from this Gram-positive species.

Previously, we reported the structure of PilJ, the first structure of a Type IV pilin from a Gram-positive organism (Piepenbrink et al., 2014). We found that PilJ has a unique fold when compared to pilin structures characterized previously, containing two pilin-like domains joined by a Cys-Cys-Cys-His-coordinated zinc atom. While immunogold staining

showed that PilJ is incorporated into the Type IV pilus of *C. difficile*, models of pilus fragments composed entirely of PilJ were significantly wider than the observed *C. difficile* Type IV pili, indicating that PilJ is a minor pilin.

Another of the Type IV pilin proteins of *C. difficile*, PilA1, is similar in size (20 kD, 164 residues for the mature protein) to the majority of previously characterized pilins. Due to its position in the primary Type IV pilus operon in the *C. difficile* genome, as well as its high degree of sequence diversity among different *C. difficile* genomes, we and others have predicted that it was the major pilin for some, if not all, of the Type IV pili expressed by *C. difficile* (Maldarelli et al., 2014; Melville and Craig, 2013; Piepenbrink et al., 2014). Here, we show that PilA1 is the major pilin for all observable *C. difficile* Type IV pili. We also present the X-ray crystal structures of PilA1 pilins from three distinct strains revealing how this protein has found more than one unique structural solution to adopting the common Type IV pilin fold. With multiple independent PilA1 structures, we show that the genetic variations in *pilA1* map to surface-exposed regions in a modeled *Clostridium difficile* Type IVb pilus.

Results

PilA1 is Required for and Composes the Majority of *Clostridium difficile* Type IV Pili

We reported previously that *Clostridium difficile* produces Type IV pili that incorporate both PilA1 and PilJ (Piepenbrink et al., 2014). Immunogold labeling revealed that several pilus fibers stained with immunogold particles corresponding to both pilins. Models of pili based on our PilJ crystal structure, however, produced pilus widths that were inconsistent with those observed by electron microscopy. Based on its size and position in the primary cluster of Type IV pilus biogenesis genes in the *C. difficile* genome, we hypothesized that PilA1 was the major pilin, composing the majority of these pili (Maldarelli et al., 2014).

By definition, the major pilin should predominate in the pili. To test the hypothesis that PilA1 is the major pilin, we used RNA-seq to measure the mRNA levels of all *C. difficile* pilin genes. As shown in Figure 1A, *pilA1* is the most highly expressed gene, several-fold more highly expressed than the next highest transcript, *pilJ*. Additionally, we used quantitative immunoblotting to measure the amount of PilA1 and PilJ protein in whole cells. These measurements, shown in Figure 1B, indicate that when grown on blood agar plates, *C. difficile* expresses 3.23 ± 1.02 nanograms of PilA1 per microgram of total protein and 1.53 ± 0.485 picograms of PilJ per microgram. This corresponds to a ratio of ~2000 molecules of PilA1 per molecule of PilJ.

To confirm these findings, we used Clostron mutagenesis to engineer a variant strain of *Clostridium difficile* R20291 deficient in PilA1. As shown in Figure 2A, numerous pili from the wild type strain are stained with gold nanoparticles for both pilins. Conversely, the *pilA1* strain produces no visible pili under conditions known to induce piliation in the wild type strain. Quantification of the immunogold staining demonstrates the absence of both PilA1 and PilJ on the surface of *C. difficile* in the *pilA1* mutant strain. The reintroduction of *pilA1* through a complementation plasmid (Dingle et al., 2011; Heap et al., 2009) restores piliation and importantly, these pili incorporate both PilA1 and PilJ as shown in Figure 2B.

Based on the sum of these factors – i) PilA1 is expressed at a much higher level than PilJ, ii) the loss of PilA1 eliminates visible piliation, and iii) the restoration of PilA1 re-incorporates PilJ into T4P – we assign PilA1 as the major pilin of all of the *C. difficile* Type IV pili that we have observed. Whether *C. difficile* can produce T4P with a different composition under other conditions remains to be seen.

The Structure of PilA1 shows remarkable conservation with Type IVb Gram-negative Pilins

We determined the 1.9Å resolution X-ray crystal structure of soluble PilA1 from *Clostridium difficile* R20291 (ribotype 027) fused to the C-terminus of Maltose Binding Protein (Table 1). PilA1 exhibits the typical pilin fold: an N-terminal α -helix, followed by a loop with some α -helical character (the α 2 helix) and then by a four-stranded anti-parallel β -sheet (Figure 3). It contains an additional α -helix (which we denote the α 3 helix) at the C-terminus and, more interestingly, a two-stranded anti-parallel β -sheet between the α 3 helix and the C-terminal strand of the central β -sheet (which we denote the B2 sheet).

The presence of a second β -sheet is not unprecedented in the structures of Type IV pilins, as the PAK pilin of *Pseudomonas aeruginosa* contains a two-strand parallel β -sheet in its $\alpha\beta$ loop and the GC pilin of *Neisseria gonorrhoeae* contains a β -hairpin in addition to the central β -sheet (Craig et al., 2003; Craig et al., 2006). However, these β structures are parallel to the central β -sheet with respect to the N-terminal α -helix. In contrast, the B2 sheet of PilA1 rests below the central β -sheet at a 90° angle to it, in an analogous position to the disulfide bond found in the vast majority of Type IV pilins from Gram-negative strains (including *N. gonorrhoeae* and *P. aeruginosa*) (Figure 3). Notably, the strands of the B2 sheet are placed at the midpoints of the β 2- β 4 and β 4- β 3 insertions in the central β -sheet (Figure 3B). We propose that the B2 sheet of PilA1 serves primarily to stabilize the C-terminus of the protein, in much the same way that the disulfide bond does in most Gram-negative pilins.

A superimposition of PilA1 with the two domains of PilJ (Figure S1) reveals considerable conservation in the N-terminal half; the α 1-C-helices, $\alpha\beta$ loops and the first two strands of each β -sheet overlay well (2.5Å RMSD). However, the C-terminal portions of PilA1 show no obvious similarity with those of either of the PilJ domains.

PilA1 and PilJ show significantly different levels of conservation

A comparison of the sequences of PilA1 and PilJ in the genomes of a large collection of *C. difficile* strains confirms our prior observation that PilA1 is much less conserved than any of the putative minor pilins (Maldarelli et al., 2014), including PilJ. Here, we have compared all of the publically available genomes of *C. difficile*, encompassing 238 strains, and found that the average variation is considerably greater in PilA1 than PilJ (Figure 4). Furthermore, using the larger data set available with newly sequenced genomes, we confirm our prior observation that residues of PilA1 are subject to diversifying selection ($p < 0.01$) (Maldarelli et al., 2014). The evidence for diversifying selection in PilJ is less clear with a p-value between 0.05 and 0.01.

Figure 4 shows the regions of conservation for PilA1 and PilJ. In both cases, the areas expected to be involved in pilus formation are conserved. In PilA1, the regions of largest variability are the loops between the strands of the β -sheet, which vary both in composition and length between the various strains of *C. difficile*. The sequences of PilJ show no insertions and only one deletion (in strain CD160) and have a much higher level of overall conservation (97% identity over 238 genomes as opposed to 90% for PilA1). As noted previously (Piepenbrink et al., 2014), the polymorphisms are primarily limited to one section of the $\alpha\beta$ loop and one face of the C-terminal domain.

The structure of PilA1 is a substantial addition to our knowledge of Type IV pilin structures because there is such great divergence between the sequences of Type IV pilins from Gram-positive and Gram-negative strains, despite the conservation of the overall fold. A recent effort to model the structure of PilA1 based on the structure of the GC pilin of *N. gonorrhoeae* correctly predicted the structure of the $\alpha\beta$ loop but was less successful in modeling the C-terminus, hindered by the low (17%) sequence identity between the two proteins (Melville and Craig, 2013). Homologs of PilA1 are found in many other Clostridiales but no homologs of PilJ are known (Figure S2).

Structural Divergence of PilA1 between *C. difficile* strains

Because of the unusual degree of sequence divergence in PilA1, at least in comparison to other *C. difficile* T4P genes, we solved the structure of PilA1 from two additional strains of *C. difficile*, NAP08 (ribotype 078) and a recently discovered divergent strain of *C. difficile* termed CD160. A sequence alignment of PilA1 from R20291, NAP08 and CD160 is shown in Figure 5A with the three regions of greatest divergence highlighted. Each of these stretches of amino acids is located within an exposed loop in the R20291 structure, leading us to hypothesize that one side of PilA1, which likely faces in towards the core of the formed pilus, would be conserved between PilA1 from different strains of *C. difficile*, while the region that likely faces out into solution would contain all significant structural differences.

Using the same crystallographic methods, we solved the structure of PilA1 from NAP08 to a resolution of 2.2Å (Table 1). As expected, the overall fold is quite similar between the two structures, with the divergent regions restricted to the face of the protein we expect to be exposed in the Type IV pilus, namely the $\alpha\beta$ loop, the loop between the second strand of the central β -sheet and the first strand of the B2 sheet, and the loop between the $\alpha 3$ helix and the second strand of the B2 sheet. (Figure 5C) These structural differences are not expected to have a significant effect on function but may well contribute to immune escape as antibodies against these regions may not be cross-protective against different strains of *C. difficile*.

We also solved the structure of PilA1 from CD160 to 1.7Å resolution (Table 1). An overlay of the R20291, NAP08 and CD160 structures is shown in Figure 5B. The overall fold of PilA1 CD160 is similar to those of R20291 and NAP08, but there are substantial differences in the loops that we expect to be exposed in the assembled pilus. In comparison to the R20291 structure, the $\alpha\beta$ loop of the CD160 structure is four residues shorter and slightly more helical and the loop between the second strand of the central β -sheet and the first strand of the B2 sheet is two residues longer and more exposed. However, the greatest

difference is in the C-terminus where the region that forms the second strand of the B2 sheet in the R20291 structure stretches farther away from the core of the protein, eliminating any possibility for direct interactions with the stretch that forms the first strand of the B2 sheet in the R20291 and NAP08 structures (Figure 5A).

This initially puzzling finding is explained by the presence of a network of water molecules between the two strands. As shown in Figure 5D, five crystallographic water molecules lie between these two strands and make hydrogen bonds to the backbone of one or both strands. Of these five waters, two in particular are highly ordered, with B-factors of 27.27 and 27.38 (the average for the structure is 33.30 overall and 38.60 for solvent atoms). Additionally, they each form one direct hydrogen bond to each strand, creating water-mediated hydrogen bonds between the two strands in place of the direct backbone-backbone hydrogen bonds of the B2 sheet found in the R20291 and NAP08 PilA1 structures (Figure S4).

The structural divergence of PilA1 from R20291, NAP08 and CD160, taken together with the structure of FimA from *Dichelobacter nodosus* (Hartung et al., 2011), show that multiple energetic strategies exist for stabilizing the C-termini of pilins in the absence of disulfide bonds. We expect that as more structures of pilins from Gram-positive species are characterized, the range of known pilin C-terminal structural motifs will continue to expand.

The Structures of PilA1 Support a Model of Pilus Formation Similar to Type IVb Pili

Previously, we found that the best model for incorporating PilJ into a Type IV pilus was based on the Toxin- Coregulated Pilus (TCP) of *V. cholerae* (Piepenbrink et al., 2014). However, the unusual dualpilin fold of PilJ complicated comparisons with other single-domain pilins. To find the closest structural analogs of PilA1, we used the DALI server (Holm and Rosenstrom, 2010); the results of that search are found in Table S1. The highest scoring matches were to TcpA of *V. cholerae* El Tor ($Z = 7.8$) and CofA of *E. coli* ($Z = 7.7$), while numerous pilins and pseudopilins were also found to have significant structural similarity including PilS from *S. Typhi*, Type 2 secretion pseudopilins GspG and EspG, and TcpA from the classical strain of *V. cholerae*.

A structural alignment of PilA1 with TcpA from the classical strain of *V. cholerae* is shown in Figure 6A. Although there are substantial differences in the folds of the two proteins, there is an obvious similarity (3.0\AA RMSD), particularly in the $\alpha\beta$ loop and in the C-terminal accessory helix (the α_3 helix of TcpA and PilA1). Based on these similarities, we modeled full-length PilA1 as previously described (Piepenbrink et al., 2014) and subsequently created a model of PilA1 pilus assembly based on the high resolution electron micrographs of the TCP (Li et al., 2008), as shown in Figure 6D. When the PilA1 pilus model was superimposed onto the TCP electron density the correlation coefficient was 0.90.

Because the structure of PilJ is also known and it is incorporated into the same Type IV pili as is PilA1 (Piepenbrink et al., 2014), we can also judge any model of PilA1 pilus formation by its ability to accommodate PilJ subunits. As shown in Figure 6D, we were able to generate models of pili composed primarily of PilA1 but with PilJ incorporated either sporadically (ii) or in stretches (iii). This was expected as a superimposition of PilA1 and PilJ (Figure 6C) shows that the two are structurally similar (RMSD = 3.65\AA) in the regions

expected to contact other pilus subunits, namely the $\alpha 1$ helix, the $\alpha\beta$ loop and the helical portion of the C-terminus.

Additionally, we noted that our model resulted in the formation of an inter-pilin salt bridge between residues Lysine 30 and Glutamate 75 of PilA1 (Figure 6B). This salt bridge was very similar in position to one shown to be important in the TCP between residues R26 and E83 (and is also found in CofA in residues R31 and E93) (Li et al., 2008). Although there is no detectable sequence similarity between PilA1 and PilJ outside of the N-terminus, PilJ contains a lysine and a glutamate in nearly identical positions when the two proteins are superimposed (Figure 6C), K30 and E76, indicating a remarkable conservation of functional residues despite complete divergence in overall sequence. In 238 genomes of *C. difficile*, the only polymorphisms found at these positions were E75D substitutions in 2% of the PilA1 sequences. To investigate the importance of this potential interaction in pilus formation by *C. difficile* we created PilA1 complementation plasmids with point mutations reversing the charges at positions 30 (K30E) and 75 (E75K). Using these plasmids to complement the *pilA1* mutant strain of *C. difficile*, we found that unlike wild type *pilA1*, the K30E and E75K mutants of *pilA1* were completely unable to produce Type IV pili (Figure 7). The double mutant *pilA1* K30E E75K was also unable to produce Type IV pili, which may stem from an imperfect recreation of the salt-bridge, but could also be due to an inability to incorporate one or more minor pilins as those proteins would not be able to form salt bridges with PilA1 K30E E75K.

Discussion

The structures of Type IV pilins from Gram-negative bacteria that have been elucidated to date are remarkable in the commonality of their folds in spite of their vast divergence in sequence. The most logical explanation for this structural conservation is a preservation of function; not that all Type IV pilins share any one function, but all share the requirement that they must be able to polymerize into pili and all of the functions ascribed to Type IV pili are related in one way or another to adhesion, be it to host cells, bacterial cells (microcolony formation), DNA (horizontal transfer) or abiotic surfaces (biofilm formation). Indeed, the division between Type IVa and Type IVb pilins is a functional one, but is represented in structural differences, particularly in the larger C-terminal loops found in Type IVb pilins (Giltner et al., 2012).

The structural similarity between PilA1 and pseudopilins is also noteworthy as pseudopilins from Gram-negative bacteria also lack a C-terminal disulfide bond and the overall similarity between Type II secretion and Type IV pili implies some common ancestral pilus-like structure. The $\alpha\beta$ loop of PilA1 resembles the variable loop of major pseudopilins in that it is largely disordered but contains some helical character in the center (Alphonse et al., 2010; Kohler et al., 2004; Korotkov et al., 2009). The placement of the calcium binding site in major pseudopilins is also similar to that of the B2 sheet of PilA1, both sequentially (it occurs in a loop between two strands of the β -sheet) and topographically (it rests below the β -sheet on an axis paralleling the $\alpha 1$ -N helix) (Giltner et al., 2012). Taken together, these data suggest that the ancestral pilin-like proteins used a variety of means to stabilize their C-terminus and that the disulfide bond became nearly ubiquitous in Type IV pilins from Gram-

negative strains as a consequence of the formation of a periplasmic space. However, this hypothesis does not explain the presence of calcium-binding motifs rather than disulfide bonds in the pseudopilins of Gram-negative Type II secretion systems.

Like other pilins identified in Gram-positive strains (Imam et al., 2011), PilA1 contains no cysteines, meaning that it lacks the ability to form the aforementioned disulfide bond. The only other known structure of a Type IV pilin without a C-terminal disulfide bond is that of FimA from *D. nodosus*, which instead contains a disulfide bond between the $\alpha\beta$ loop and the third strand of its β -sheet, and is proposed to use a combination of hydrogen bonds and hydrophobic interactions to stabilize its C-terminus (Hartung et al., 2011). However, unlike FimA, which is a Type IVa pilin and has a continuous β -sheet with relatively short sequences between the strands, PilA1 has a discontinuous β -sheet. The C-terminal β -strand is not the final strand, but instead the $\alpha 3$ helix, the final (fourth) β -strand and the B2 sheet are placed sequentially between the second and third strands; analogous to what is seen in the Type IVb pilins, including TcpA from *Vibrio cholerae*, CofA from enterotoxigenic *Escherichia coli* (ETEC) and PilS from *S. typhi* (Balakrishna et al., 2009; Craig et al., 2003; Kolappan et al., 2012). This leaves a 34-residue loop between the second and fourth strands of the central β -sheet.

The obvious question arises: How then does PilA1 stabilize its C-terminus? The near-universal frequency of the C-terminal disulfide bond in Type IV pilins from Gram-negative species has long been considered an indication of its importance (Giltner et al., 2012). However, its absence in Gram-positive Type IV pilins shows that FimA is part of a larger pattern of Type IV pilins in which non-covalent interactions are used in place of a covalent disulfide bond at the C-terminus of the protein.

One possible explanation can be found by comparing the C-terminus of PilA1 to other Type IV pilins. The C-termini are the least conserved regions of Type IV pilins and we expect that they will vary considerably in terms of the strength of the interactions needed to anchor C-terminal loops to the core of the protein. Figure S5 shows the C-terminal structures of various Type IV pilins and pseudopilins. The disulfide bonds of PilE and PilA (PAK) anchor C-terminal loops to their β -sheets, while the disulfide bonds of TcpA, PilS and CofA bridge two C-terminal α -helices found in loops between the strands of the β -sheet (Giltner et al., 2012). The PilA1 fold contains the discontinuous β -sheet found in Type IVb pilins but it contains only one C-terminal α -helix, making PilA1 more compact than the Gram-negative pilins that it most closely resembles. This more compact fold leaves only two long insertions between the strands of the central β -sheet and each of them contains one strand of the B2 sheet, anchoring the extended $\beta 4$ - $\beta 3$ loop to the core of the protein.

That same portion of the $\beta 4$ - $\beta 3$ loop in PilA1 CD160 extends outward, dissolving the B2 sheet and creating a network of water-mediated hydrogen bonds in its place. This alternate conformation alters the surface of PilA1 significantly, which is likely to affect both function and immune recognition, although all three forms of PilA1 are stabilized by hydrogen bonds between the $\beta 2$ - $\beta 4$ and $\beta 4$ - $\beta 3$ loops.

The structure of the *C. difficile* minor pilin, PilJ, demonstrated how far a pilin can deviate from these established norms while maintaining the ability to incorporate into a Type IV pilus (Piepenbrink et al., 2014). But the structure of the major pilin of *C. difficile*, PilA1, allows for a better comparison to the structures of major pilins from other species. All of the structures of PilA1 presented here show a similar overall shape to PilS (*S. typhi*), TcpA (*V. cholerae*) and CofA (ETEC), including a helical region in the C-terminus that superimposes onto the $\alpha 3$ helix of TcpA. Despite the overall differences in fold, PilJ also has a helical region that superimposes onto the same $\alpha 3$ region. Additionally, TcpA, CofA, PilJ and PilA1 share a pair of residues in similar positions that we expect form a salt bridge in all three pili.

The Type IV pili of Gram-positive species are as yet only sparsely characterized, but a recent review noted the similarities in genetic organization between clostridial pilus biogenesis machinery and the Type IVb pilus operons (Melville and Craig, 2013). Here, we show that the structures of two Type IV pilins from *Clostridium difficile* show a remarkable resemblance to Type IVb pilins in the width of their head groups, the relative positions of helical regions and in the configuration of the central β -sheet of the major pilin, PilA1.

While Type IVb pili have been implicated in a variety of functions, the most common is microcolony formation, which has been demonstrated to occur through Type IV pilus bundling in EPEC and *S. typhi* (Bieber et al., 1998; Raza et al., 2011). If we examine those Type IV pilus systems most closely related to the *C. difficile* pili by the structures of their major pilins, we find that the Type IV pili of *V. cholera*, *S. typhi* and ETEC have all been implicated in microcolony formation (Clavijo et al., 2010; Tam et al., 2006). As *C. difficile* is known to colonize the human intestine and has been observed to form microcolonies in a hamster model (Buckley et al., 2011), which appear to be mediated by “flagella-like appendages” resembling Type IV pili, it is likely that one function of Type IV pili in *C. difficile* is to mediate this self-association in vivo.

The function of PilJ within the Type IV pili of *C. difficile* also remains to be determined. Although hypotheses are somewhat speculative at this juncture, the fact that PilJ has so much more exposed surface area in our model of the pilus and its low incorporation rate suggest that it does not significantly aid in stabilizing the pilus but rather serves as an adhesin.

In conclusion, while the role of Type IV pili in the colonization and pathogenic strategies of *C. difficile* remains to be determined, the fold of PilA1 shows the flexibility of the Type IV pilin architecture and the variety of structural motifs that can be used to form similar folds. This flexibility allows for substantial variation in the sequence of the pilin head-groups while maintaining an immediately recognizable common protein fold.

Experimental Procedures

Reagents

Polyclonal anti-sera against PilA1 and PilJ used in this study were generated using recombinant proteins as described previously (Maldarelli et al., 2014; Piepenbrink et al., 2014).

Protein expression and purification

The codon-optimized sequences of PilA1 from strains R20291, NAP08 and CD160, starting with Serine 26, were cloned into a Maltose Binding Fusion vector making use of previously described surface entropy reduction mutations (pMal E) (Moon et al., 2010). A C-terminal 6xHIS tag was included for ease of purification. These clones were transformed into BL21 (DE3) pLysS cells and grown to saturation overnight with shaking at 37C in LB media with 50ug/ml ampicillin. These saturation cultures were then diluted into fresh LB-ampicillin and grown to and OD of 0.4–0.6 at 37C. These flasks were transferred to a refrigerated orbital shaker and cooled to 18C before induction with 30 μ M Isopropyl α -D-1-thiogalactopyranoside (IPTG). These flasks were allowed to grow overnight before being harvested by centrifugation at 7500 x g for ten minutes. The cells were then lysed using lysozyme and the resulting lysate centrifuged again, this time at 20000 x g for 30 minutes. The supernatant was purified using a nickel-NTA column and the elution further purified through size exclusion chromatography over a GE S200 superdex column using an Åkta purifier FPLC.

Structure Determination and Refinement

All three MBP-PilA1 constructs were initially screened at a concentration of 20 mg/ml in 20 mM Bis-tris pH 6.0, 100 mM NaCl, 50 mM Maltose. However, each crystallized in a different set of precipitating conditions and optimization produced different ideal concentrations of NaCl and Maltose.

NAP08—MBP-PilA1 NAP08 initially crystallized in Hampton's Index screen condition D7 (25% PEG 3350, 100 mM Bis-tris pH 6.5) at room temperature. The optimal buffer conditions were 20 mM Bis-tris pH 6.0, 100mM NaCl and the optimal precipitant conditions were 25% PEG 2000MME, 100 mM Bis-tris pH 6.5 (crystals were grown by hanging drop vapor diffusion at 4C). Crystals grew overnight and were harvested and flash-cooled in the mother liquor supplemented with 25% glycerol. Data were collected at the National Light Source in Brookhaven, NY, Beamline x25.

CD160—MBP-PilA1 CD160 initially crystallized in Emerald Biosystems Wizard III/IV F12 (2.4 M Sodium Malonate). The optimal buffer conditions were 20 mM Bis-tris pH 6.0, 100 mM NaCl, 100 mM Maltose, optimization did not change the precipitant conditions (crystals were grown by sitting drop vapor diffusion at room temperature). Crystals grew overnight and were harvested and flash-cooled without the addition of any additional cryo-protectant. Data were collected remotely at Stanford Synchrotron Radiation Labs (SSRL) beamline 12-2.

To ensure that the alternate conformation found in the CD160 structure is not a crystallographic artifact of the I 1 2 1 space group, which has close crystal contacts in this region of the protein, we also solved the structure in a different crystal form (space group: P 1 21 1), which has no crystal contacts in this region. The structures of CD160 PilA1 in these two crystal structures were found to be essentially identical and density for crystallographic waters was found in nearly identical positions in the space between the two B2 strands.

R20291—MBP-PilA1 R20291 Emerald Biosystems Wizard I/II B9 (20% PEG 8000, 100 mM HEPES pH 7.5). The optimal concentration was 30 mg/ml and the optimal buffer conditions 20 mM Bis-tris pH 6.0, 50mM Maltose, optimization did not change the precipitant conditions (crystals were grown by hanging drop vapor diffusion at room temperature).

All three datasets were processed with XDS (Kabsch, 2010). Molecular replacement was carried out by Phaser (McCoy et al., 2007) using Maltose Binding Protein (MBP-PilA1 NAP08) or a sequential search of 1) Maltose Binding Protein and 2) PilA1 NAP08 (MBP-PilA1 CD160 and MBP-PilA1 R20291). Phenix and Coot were used for phasing, building and refinement (Adams et al., 2010; Adams et al., 2011; Adams et al., 2002; Emsley and Cowtan, 2004). Multiple iterative rounds of model building and refinement resulted in an Rwork factor of 20.1% and an Rfree of 24.7% (NAP08), an Rwork factor of 19.7% and Rfree of 22.2% (CD160) and an Rwork factor of 19.7% and Rfree of 23.3% (R20291). The crystallographic parameters of the refined data are summarized in Table 1.

C. difficile lysate preparation

Cultures of *C. difficile* strain R20291 were grown on Columbia agar plates as above. Colonies were scraped off plates, resuspended in PBS, and brought to an OD600 of 20. Bacteria were lysed as described previously (Lawley et al., 2009); briefly, resuspended cells were frozen at -20°C overnight, then incubated at 37°C for 40 minutes. Total protein present in each lysate was quantified with a commercial bichinoic acid (BCA) assay kit (Thermo Scientific Pierce) according to the manufacturer's protocol.

In preparation for immunoblotting, lysates were diluted 1:1 in Laemmli buffer and boiled for 10 minutes. Lysates and a standard curve of purified untagged PilJ and PilA1 were separated on precast 4–15% gradient Mini-PROTEAN TGX polyacrylamide gels (Bio-Rad) and transferred to polyvinylidene difluoride (PVDF) membranes. Blots were blocked for 1 hour with 5% non-fat dry milk, then incubated at 4°C overnight with polyclonal rabbit anti-PilJ at a 1:10,000 dilution. Blots were washed in PBST, incubated with IRDye 800CW donkey anti-rabbit IgG H+L (Li-Cor Biosciences) at a 1:20,000 dilution for 1 hour. Infrared signals were detected and quantified using the Odyssey imaging system (Li-Cor Biosciences).

Creation of *C. difficile* pilA1 gene interruption mutant

C. difficile mutants were produced using the ClosTron system (Heap et al., 2010). Retargeted MTL007C-E2 vectors for the *Cdi-pilA1-39a* mutant was purchased from DNA2.0 Inc. The retargeted vector was transferred from *Escherichia coli* CA434 to wild-

type R20291 *C. difficile* by conjugation using CCFA plates containing 15 mg/ml thiamphenicol. Once colonies appeared on the plates (48 to 72 h), they were restreaked onto CCFA containing 2.5 µg/ml erythromycin to select for bacteria in which the intron had been inserted. Insertions were confirmed by PCR using the EBS universal primer (5' cgaattagaaactgcgttcagtaaac) and a reverse primer (*pilAIF*, 5' ccttgccggcgcgcagatagataaacagtgttct).

Creation of *C. difficile* *pilA1*, *pilA1K30E*, *pilA1E75K* and *pilA1K30E-E75K* complemented strains

To complement the *pilA1* mutation, the *pilA1* gene and its promoter region were PCR amplified using the above indicated primer *pilAIF* and the *pilAIR* (5' ccctgctcgagctat tttgttgagtcacac) and cloned into the p84151 modular plasmid using the *NotI* and *XhoI* restriction enzymes (Heap et al., 2009). The vector was then transformed into *E. coli* CA434 and conjugated into *Cdi-pilA1-39a*, and positive conjugants were selected for on CCFA containing 15 µg/mL thiamphenicol. Complement strains were screened by PCR and western immunoblotting to confirm the proper genotype and phenotype.

For the construction of the complementation plasmids *pilA1K30E*, *pilA1E75K* and *pilA1K30EE75K* we used the Quick Change Mutagenesis system (Agilent Technologies) using the p84151-*pilA1* as a template and the primers *pilA1K30EF* (5' cca gct tta ttt agt aat ata aac gaa gct aag gta gca agt gtt gag tct g), *pilA1k30ER* (5' cag act caa cac ttg cta cct tag ctg cgt tta tat tac taa ata aag ctg g), *pilA1E75K* fF (5' gtg ttt tag aga ctt ata tga aat ctc tgc ctg ata aag ctg), *pilA1E75KR* (5' cag ctt tat cag gca gag att tca tat aag tct cta aaa cac) to introduce the mutations in the desire codons. The resultant plasmids were confirmed by sequencing and transformed into CA434 for posterior conjugation with the *Cdi-pilA1-39a* mutant.

Immunogold Electron Microscopy

The immunogold EM assays were performed as described in Piepenbrink *et al* (Piepenbrink et al., 2014).

Genetic Analysis

Protein sequences of PilA1 and PilJ were translated from *C. difficile* genome sequences in the NCBI database, were aligned with ClustalX (Jeanmougin et al., 1998) and analyzed using SAIS and Bioedit.

RNA Seq

Cultures of *C. difficile* strain R20291 were grown on Columbia agar plates as above. Within an anaerobic chamber (Coy Laboratories, Grass Lake, MI), colonies were removed and placed immediately into RNAProtect™ bacteria reagent (Qiagen) and stored at -80°C until used. After thawing, cells were pelleted and resuspended in 100 µL TES buffer with 35,000 units of Ready-Lyse™ lysozyme solution (Epicentre Technologies, Madison, WI) and incubated with shaking at room temperature for 90 minutes. The RNeasy™ RNA purification kit (Qiagen) was then used per the manufacturer's instructions. RNA quantity and integrity were measured with an Agilent bioanalyzer and all RNA integrity numbers (RIN) exceeded eight. Total RNA samples were treated with DNase I (Invitrogen). The level

of ribosomal RNA present in total RNA samples was reduced prior to library construction using the Ribo-Zero™ Gram Positive Bacteria rRNA Removal Kit (Epicentre Technologies, Madison, WI). Illumina RNA-seq libraries were prepared with the TruSeq RNA Sample Prep kit (Illumina, San Diego, CA), omitting the poly-A selection steps. Adapters containing six-nucleotide indexes were ligated to the double-stranded cDNA. The DNA was purified between enzymatic reactions and the size selection of the library was performed with AMPure XT beads (Beckman Coulter Genomics, Danvers, MA). The libraries were sequenced on a 100 bp paired end run on the HiSeq 2000 (Illumina, San Diego, CA).

Pilus Modelling

Full-length PilA1 and PilJ were modelled using the structure of the full-length *Pseudomonas aeruginosa* PAK pilin (Craig et al., 2003). The initial model of the PilA1 pilus was created by superimposition onto a model of the Toxin-coregulated pilus of *V. cholerae* (PDBID: 1OR9), which did not result in any clashes. The resulting model then underwent rigid-body minimization by UCSF Chimera (Pettersen et al., 2004) using the electron density from a high-resolution cryo-EM micrograph of the TCP (EMD-1954). The incorporation of PilJ was modelled by replacing PilA1 subunits with superimposed PilJ subunits without additional refinement.

Supplementary Material

Refer to Web version on PubMed Central for supplementary material.

Acknowledgments

This work was supported by National Institutes of Health grant R21 AI105881 (to M.S.D.). Additional work was supported by the Alberta Glycomics Centre. K.H.P. was supported in part by National Institutes of Health training grant T32 AI095190 and by an NIH fellowship NIH F32 AI 110045. C.M.P. was supported in part by Mexico's National Council for Science and Technology No. 130211 (CONACYT).

We thank the staff at Brookhaven National Laboratory National Synchrotron Light Source beam line X25 and the staff at Stanford Synchrotron Radiation Lightsource beam line 12-2 for technical assistance with X-ray data collection. We also thank Alison Scott for technical assistance in collecting and analyzing the RNA-Seq data.

References

- Adams PD, Afonine PV, Bunkoczi G, Chen VB, Davis IW, Echols N, Headd JJ, Hung LW, Kapral GJ, Grosse-Kunstleve RW, et al. PHENIX: a comprehensive Python-based system for macromolecular structure solution. *Acta Crystallogr D Biol Crystallogr*. 2010; 66:213–221. [PubMed: 20124702]
- Adams PD, Afonine PV, Bunkoczi G, Chen VB, Echols N, Headd JJ, Hung LW, Jain S, Kapral GJ, Grosse Kunstleve RW, et al. The Phenix software for automated determination of macromolecular structures. *Methods*. 2011; 55:94–106. [PubMed: 21821126]
- Adams PD, Grosse-Kunstleve RW, Hung LW, Ioerger TR, McCoy AJ, Moriarty NW, Read RJ, Sacchettini JC, Sauter NK, Terwilliger TC. PHENIX: building new software for automated crystallographic structure determination. *Acta Crystallogr D Biol Crystallogr*. 2002; 58:1948–1954. [PubMed: 12393927]
- Alphonse S, Durand E, Douzi B, Waegle B, Darbon H, Filloux A, Voulhoux R, Bernard C. Structure of the *Pseudomonas aeruginosa* XcpT pseudopilin, a major component of the type II secretion system. *J Struct Biol*. 2010; 169:75–80. [PubMed: 19747550]

- Balakrishna AM, Saxena AM, Mok HY, Swaminathan K. Structural basis of typhoid: Salmonella typhi type IVb pilin (PilS) and cystic fibrosis transmembrane conductance regulator interaction. *Proteins*. 2009; 77:253–261. [PubMed: 19626704]
- Bieber D, Ramer SW, Wu CY, Murray WJ, Tobe T, Fernandez R, Schoolnik GK. Type IV pili, transient bacterial aggregates, and virulence of enteropathogenic *Escherichia coli*. *Science*. 1998; 280:2114–2118. [PubMed: 9641917]
- Borriello SPD, HA, Barclay FE. Detection of fimbriae amongst strains of *Clostridium difficile*. *Fems Microbiol Lett*. 1988; 49:65–67.
- Bradley DE. A function of *Pseudomonas aeruginosa* PAO polar pili: twitching motility. *Can J Microbiol*. 1980; 26:146–154. [PubMed: 6105908]
- Buckley AM, Spencer J, Candlish D, Irvine JJ, Douce GR. Infection of hamsters with the UK *Clostridium difficile* ribotype 027 outbreak strain R20291. *J Med Microbiol*. 2011; 60:1174–1180. [PubMed: 21330415]
- Clavijo AP, Bai J, Gomez-Duarte OG. The Longus type IV pilus of enterotoxigenic *Escherichia coli* (ETEC) mediates bacterial self-aggregation and protection from antimicrobial agents. *Microb Pathog*. 2010; 48:230–238. [PubMed: 20227481]
- Craig L, Pique ME, Tainer JA. Type IV pilus structure and bacterial pathogenicity. *Nature reviews Microbiology*. 2004; 2:363–378.
- Craig L, Taylor RK, Pique ME, Adair BD, Arvai AS, Singh M, Lloyd SJ, Shin DS, Getzoff ED, Yeager M, et al. Type IV pilin structure and assembly: X-ray and EM analyses of *Vibrio cholerae* toxin-coregulated pilus and *Pseudomonas aeruginosa* PAK pilin. *Mol Cell*. 2003; 11:1139–1150. [PubMed: 12769840]
- Craig L, Volkman N, Arvai AS, Pique ME, Yeager M, Egelman EH, Tainer JA. Type IV pilus structure by cryo-electron microscopy and crystallography: implications for pilus assembly and functions. *Mol Cell*. 2006; 23:651–662. [PubMed: 16949362]
- Dingle TC, Mulvey GL, Armstrong GD. Mutagenic analysis of the *Clostridium difficile* flagellar proteins, FliC and FliD, and their contribution to virulence in hamsters. *Infect Immun*. 2011; 79:4061–4067. [PubMed: 21788384]
- Emsley P, Cowtan K. Coot: model-building tools for molecular graphics. *Acta Crystallogr D Biol Crystallogr*. 2004; 60:2126–2132. [PubMed: 15572765]
- Giltner CL, Nguyen Y, Burrows LL. Type IV pilin proteins: versatile molecular modules. *Microbiology and molecular biology reviews : MMBR*. 2012; 76:740–772. [PubMed: 23204365]
- Giron JA, Ho ASY, Schoolnik GK. An Inducible Bundle-Forming Pilus of Enteropathogenic *Escherichia-Coli*. *Science*. 1991; 254:710–713. [PubMed: 1683004]
- Goulding D, Thompson H, Emerson J, Fairweather NF, Dougan G, Douce GR. Distinctive profiles of infection and pathology in hamsters infected with *Clostridium difficile* strains 630 and B1. *Infect Immun*. 2009; 77:5478–5485. [PubMed: 19752031]
- Hartung S, Arvai AS, Wood T, Kolappan S, Shin DS, Craig L, Tainer JA. Ultrahigh resolution and full-length pilin structures with insights for filament assembly, pathogenic functions, and vaccine potential. *J Biol Chem*. 2011; 286:44254–44265. [PubMed: 22027840]
- Heap JT, Kuehne SA, Ehsaan M, Cartman ST, Cooksley CM, Scott JC, Minton NP. The ClosTron: Mutagenesis in *Clostridium* refined and streamlined. *J Microbiol Meth*. 2010; 80:49–55.
- Heap JT, Pennington OJ, Cartman ST, Minton NP. A modular system for *Clostridium* shuttle plasmids. *J Microbiol Methods*. 2009; 78:79–85. [PubMed: 19445976]
- Henrichsen J. Twitching motility. *Ann Rev Microbiol*. 1983; 37:81–93. [PubMed: 6139059]
- Herrington DA, Hall RH, Losonsky G, Mekalanos JJ, Taylor RK, Levine MM. Toxin, Toxin-Coregulated Pili, and the ToxR Regulon Are Essential for *Vibrio-Cholerae* Pathogenesis in Humans. *J Exp Med*. 1988; 168:1487–1492. [PubMed: 2902187]
- Holm L, Rosenstrom P. Dali server: conservation mapping in 3D. *Nucleic Acids Res*. 2010; 38:W545–549. [PubMed: 20457744]
- Imam S, Chen Z, Roos DS, Pohlschroder M. Identification of surprisingly diverse type IV pili, across a broad range of gram-positive bacteria. *PLoS One*. 2011; 6:e28919. [PubMed: 22216142]
- Jeanmougin F, Thompson JD, Gouy M, Higgins DG, Gibson TJ. Multiple sequence alignment with Clustal X. *Trends Biochem Sci*. 1998; 23:403–405. [PubMed: 9810230]

- Kabsch W. Xds. *Acta Crystallogr D Biol Crystallogr*. 2010; 66:125–132. [PubMed: 20124692]
- Kohler R, Schafer K, Muller S, Vignon G, Diederichs K, Philippsen A, Ringler P, Pugsley AP, Engel A, Welte W. Structure and assembly of the pseudopilin PulG. *Mol Microbiol*. 2004; 54:647–664. [PubMed: 15491357]
- Kolappan S, Roos J, Yuen AS, Pierce OM, Craig L. Structural characterization of CFA/III and Longus type IVb pili from enterotoxigenic *Escherichia coli*. *J Bacteriol*. 2012; 194:2725–2735. [PubMed: 22447901]
- Korotkov KV, Gray MD, Kreger A, Turley S, Sandkvist M, Hol WG. Calcium is essential for the major pseudopilin in the type 2 secretion system. *J Biol Chem*. 2009; 284:25466–25470. [PubMed: 19640838]
- Laurenceau R, Pehau-Arnaudet G, Baconnais S, Gault J, Malosse C, Dujeancourt A, Campo N, Chamot-Rooke J, Le Cam E, Claverys JP, et al. A type IV pilus mediates DNA binding during natural transformation in *Streptococcus pneumoniae*. *Plos Pathog*. 2013; 9:e1003473. [PubMed: 23825953]
- Lawley TD, Croucher NJ, Yu L, Clare S, Sebahia M, Goulding D, Pickard DJ, Parkhill J, Choudhary J, Dougan G. Proteomic and genomic characterization of highly infectious *Clostridium difficile* 630 spores. *J Bacteriol*. 2009; 191:5377–5386. [PubMed: 19542279]
- Lee KK, Sheth HB, Wong WY, Sherburne R, Paranchych W, Hodges RS, Lingwood CA, Krivan H, Irvin RT. The binding of *Pseudomonas aeruginosa* pili to glycosphingolipids is a tip-associated event involving the C-terminal region of the structural pilin subunit. *Mol Microbiol*. 1994; 11:705–713. [PubMed: 7910938]
- Li J, Lim MS, Li S, Brock M, Pique ME, Woods VL Jr, Craig L. *Vibrio cholerae* toxin-coregulated pilus structure analyzed by hydrogen/deuterium exchange mass spectrometry. *Structure*. 2008; 16:137–148. [PubMed: 18184591]
- Maldarelli GA, De Masi L, von Roseninge EC, Carter M, Donnenberg MS. Identification, immunogenicity, and cross-reactivity of type IV pilin and pilin-like proteins from *Clostridium difficile*. *Pathogens and disease*. 2014
- McCoy AJ, Grosse-Kunstleve RW, Adams PD, Winn MD, Storoni LC, Read RJ. Phaser crystallographic software. *J Appl Crystallogr*. 2007; 40:658–674. [PubMed: 19461840]
- Melville S, Craig L. Type IV Pili in Gram-Positive Bacteria. *Microbiology and molecular biology reviews* : MMBR. 2013; 77:323–341. [PubMed: 24006467]
- Merz AJ, So M, Sheetz MP. Pilus retraction powers bacterial twitching motility. *Nature*. 2000; 407:98–102. [PubMed: 10993081]
- Moon AF, Mueller GA, Zhong X, Pedersen LC. A synergistic approach to protein crystallization: combination of a fixed-arm carrier with surface entropy reduction. *Protein science : a publication of the Protein Society*. 2010; 19:901–913. [PubMed: 20196072]
- O'Toole GA, Kolter R. Flagellar and twitching motility are necessary for *Pseudomonas aeruginosa* biofilm development. *Mol Microbiol*. 1998; 30:295–304. [PubMed: 9791175]
- Pettersen EF, Goddard TD, Huang CC, Couch GS, Greenblatt DM, Meng EC, Ferrin TE. UCSF Chimera--a visualization system for exploratory research and analysis. *J Comput Chem*. 2004; 25:1605–1612. [PubMed: 15264254]
- Piepenbrink KH, Maldarelli GA, de la Pena CF, Mulvey GL, Snyder GA, De Masi L, von Roseninge EC, Gunther S, Armstrong GD, Donnenberg MS, et al. Structure of *Clostridium difficile* PilJ exhibits unprecedented divergence from known type IV pilins. *J Biol Chem*. 2014; 289:4334–4345. [PubMed: 24362261]
- Rakotoarivonina H, Jubelin G, Hebraud M, Gaillard-Martinie B, Forano E, Mosoni P. Adhesion to cellulose of the Gram-positive bacterium *Ruminococcus albus* involves type IV pili. *Microbiology*. 2002; 148:1871–1880. [PubMed: 12055307]
- Raza A, Sarwar Y, Ali A, Jamil A, Haque A, Haque A. Effect of biofilm formation on the excretion of *Salmonella enterica* serovar Typhi in feces. *Int J Infect Dis*. 2011; 15:e747–752. [PubMed: 21816646]
- Rudel T, Scheurerpflug I, Meyer TF. *Neisseria* PilC protein identified as type-4 pilus tip-located adhesin. *Nature*. 1995; 373:357–359. [PubMed: 7830772]

- Seifert HS, Ajioka RS, Marchal C, Sparling PF, So M. DNA transformation leads to pilin antigenic variation in *Neisseria gonorrhoeae*. *Nature*. 1988; 336:392–395. [PubMed: 2904127]
- Stone BJ, Abu Kwaik Y. Expression of multiple pili by *Legionella pneumophila*: identification and characterization of a type IV pilin gene and its role in adherence to mammalian and protozoan cells. *Infect Immun*. 1998; 66:1768–1775. [PubMed: 9529112]
- Strom MS, Lory S. Structure-function and biogenesis of the type IV pili. *Annu Rev Microbiol*. 1993; 47:565–596. [PubMed: 7903032]
- Tacket CO, Taylor RK, Losonsky G, Lim Y, Nataro JP, Kaper JB, Levine MM. Investigation of the roles of toxin-coregulated pili and mannose-sensitive hemagglutinin pili in the pathogenesis of *Vibrio cholerae* O139 infection. *Infect Immun*. 1998; 66:692–695. [PubMed: 9453628]
- Tam CK, Morris C, Hackett J. The *Salmonella enterica* serovar Typhi type IVB self-association pili are detached from the bacterial cell by the PilV minor pilus proteins. *Infect Immun*. 2006; 74:5414–5418. [PubMed: 16926438]
- Taniguchi T, Fujino Y, Yamamoto K, Miwatani T, Honda T. Sequencing of the gene encoding the major pilin of pilus colonization factor antigen III (CFA/III) of human enterotoxigenic *Escherichia coli* and evidence that CFA/III is related to type IV pili. *Infect Immun*. 1995; 63:724–728. [PubMed: 7822050]
- Varga JJ, Nguyen V, O'Brien DK, Rodgers K, Walker RA, Melville SB. Type IV pili-dependent gliding motility in the Gram-positive pathogen *Clostridium perfringens* and other *Clostridia*. *Mol Microbiol*. 2006; 62:680–694. [PubMed: 16999833]
- Wall D, Kaiser D. Type IV pili and cell motility. *Mol Microbiol*. 1999; 32:1–10. [PubMed: 10216854]
- Yoshida T, Kim SR, Komano T. Twelve pil genes are required for biogenesis of the R64 thin pilus. *J Bacteriol*. 1999; 181:2038–2043. [PubMed: 10094679]
- Zhang XL, Tsui ISM, Yip CMC, Fung AWY, Wong DKH, Dai XY, Yang YH, Hackett J, Morris C. *Salmonella enterica* serovar Typhi uses type IVB pili to enter human intestinal epithelial cells. *Infect Immun*. 2000; 68:3067–3073. [PubMed: 10816445]

Highlights

- PilA1 is the major pilin of the Type IV pili (T4P) in *C. difficile*.
- *C. difficile* strains show distinct stabilization strategies in the fold of PilA1.
- PilA1 structural similarity to the Type IVb pili of Gram-negative bacteria.
- Both PilA1 and PilJ are incorporated into T4P through an inter-subunit salt-bridge.

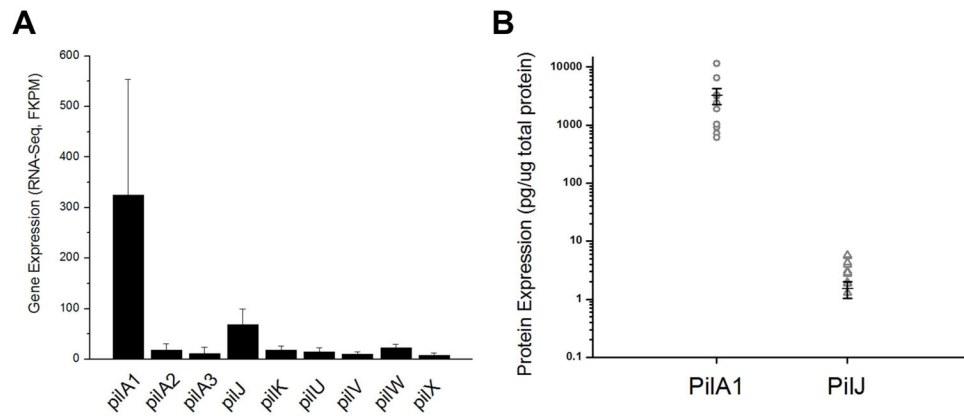


Figure 1. Expression of PilA1 and PilJ

A) mRNA expression of putative pilin genes in *C. difficile*. Average mRNA levels are shown for each protein with error bars indicating the standard deviation. B) Protein expression of PilA1 and PilJ in *C. difficile*. Expression levels from multiple independent experiments are plotted on a logarithmic scale with the error bars indicating the standard error.

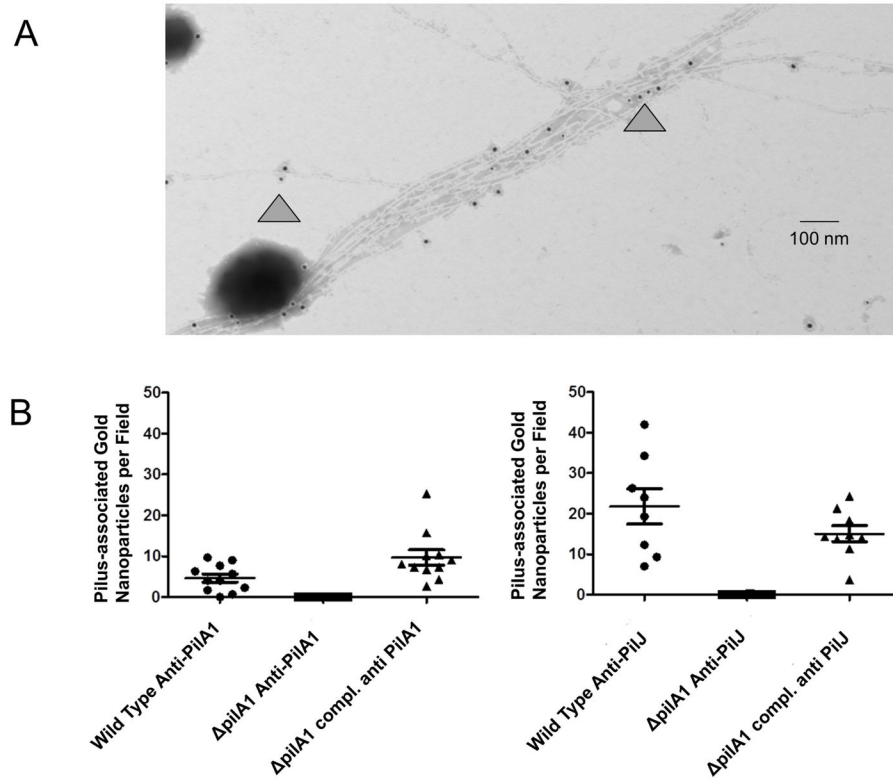


Figure 2. Type IV Pilus Expression in *Clostridium difficile*

A) Immunogold electron microscopy of *C. difficile*. Electron micrographs were stained with anti-PilA1 and anti-PilJ antibodies and immunogold-labeled secondary antibodies with particle sizes 10nm (PilA1) and 15nm (PilJ). Co-localized 10nm and 15nm particles are indicated with triangles. B) Quantification of immunogold labeling. The average number of particles per field is shown as a horizontal line. The error bars show one standard deviation.

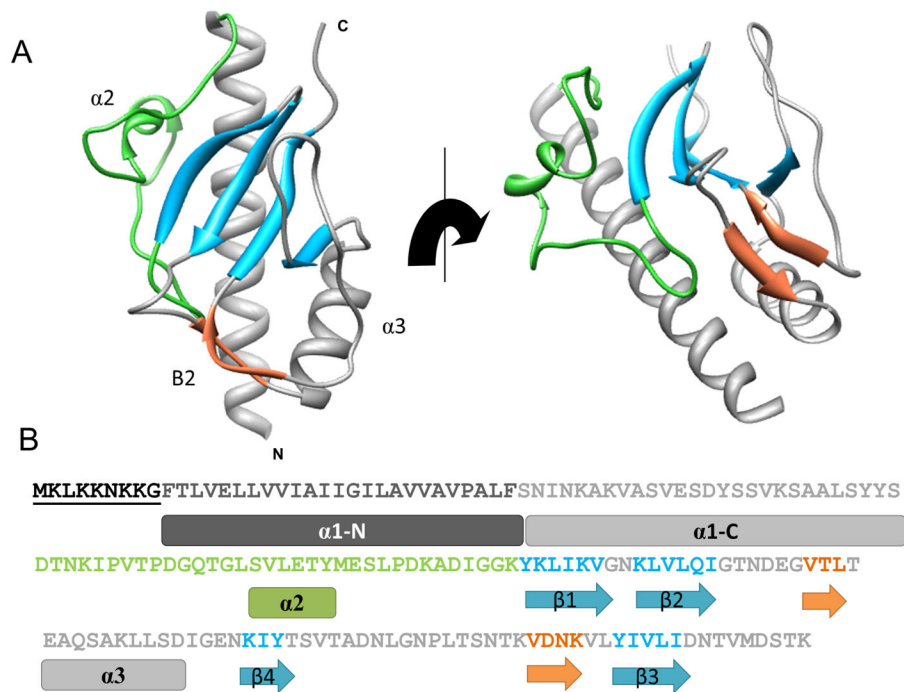


Figure 3. PilA1 Three-Dimensional Structure

A) Three-dimensional structure of PilA1 from *C. difficile* R20291. The $\alpha\beta$ loop is shown in green and the central beta sheet in blue. The B2 sheet is depicted in orange. B) Schematic diagram of PilA1 secondary structure. The prepilin leader sequence is underlined and the α -1N helix is colored dark grey. The head group is colored grey save for the $\alpha\beta$ loop and the two beta sheets which are colored to match those in 3A.

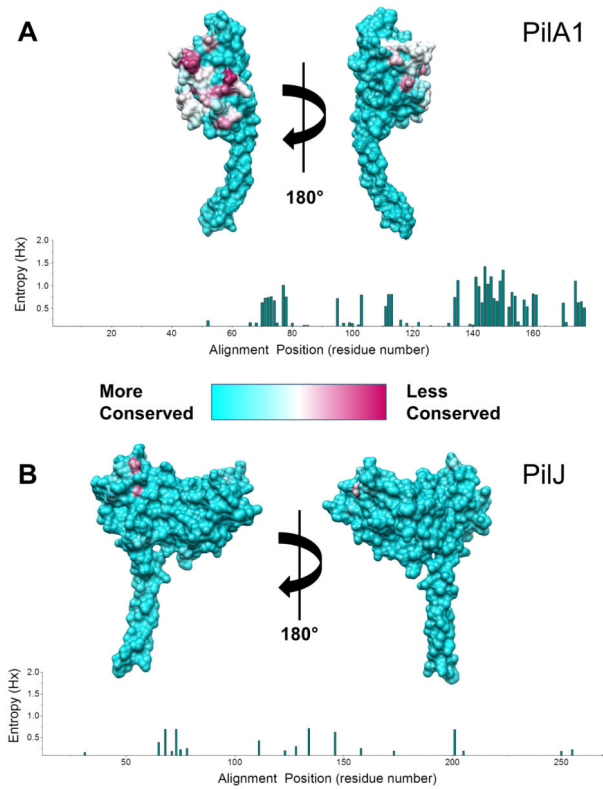


Figure 4. Genetic Analysis of *C. difficile* Type IV Pilins

Conservation heat-maps of the PilA1 and PilJ three-dimensional structures showing regions of conservation in cyan and variable regions in maroon. Below, Shannon Entropy plots (BioEdit) show the degree of sequence variability at each position.

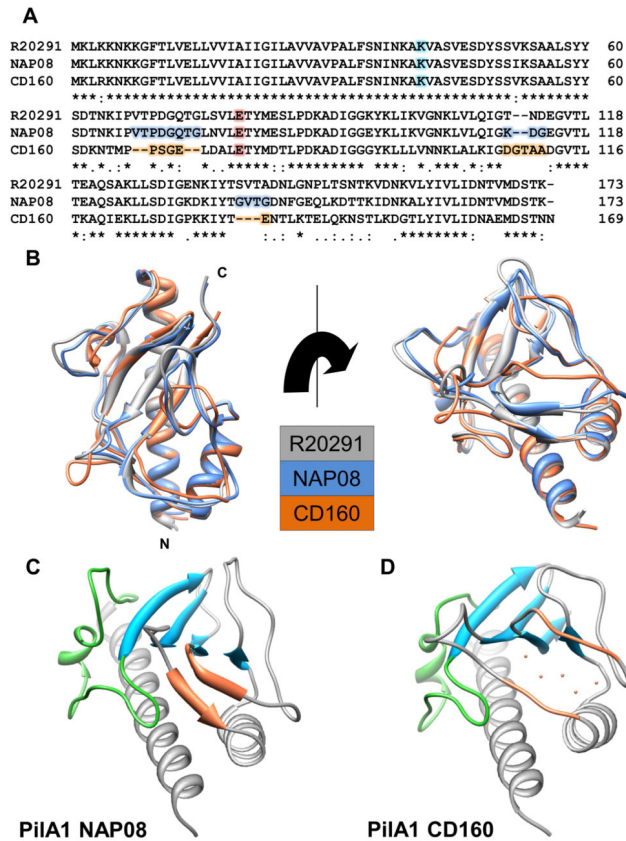


Figure 5. Variability in PilA1 Sequence and Structure

A) Sequence alignment of PilA from *C. difficile* R20291, NAP08 and CD160. Lysine 30 and Glutamate 75 are highlighted in blue and red respectively. Three variable loops are also highlighted. B) Overlay of the three dimensional structures of PilA1 from *C. difficile* R20291 (gret), NAP08 (blue) and CD160 (orange). C) Three-dimensional structure of PilA1 NAP08 and D) Three-dimensional structure of PilA1 CD160. The $\alpha\beta$ loop is shown in green and the central beta sheet in blue. The strands which make up the B2 sheet in the R20291 and NAP08 structures are depicted in orange, as are the water molecules forming water-mediated hydrogen bonds between the two strands in CD160.

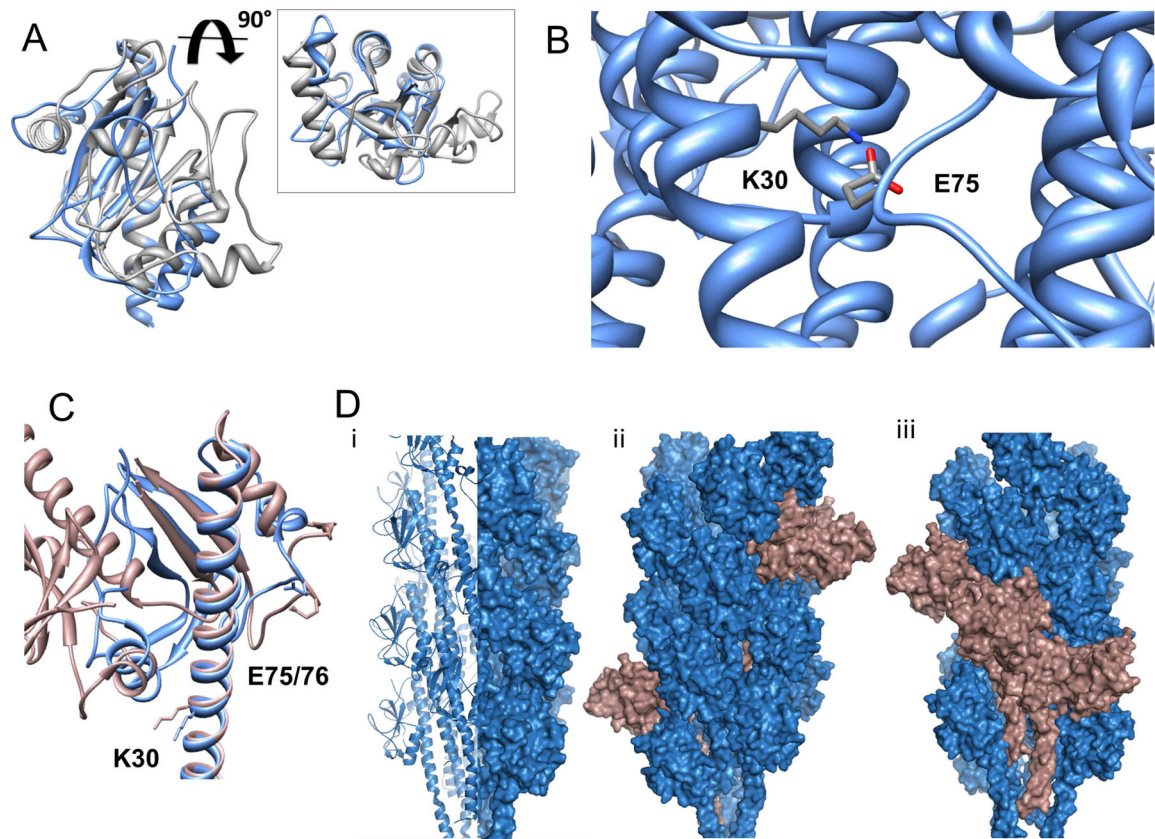


Figure 6. Incorporation of PilA1 and PilJ into T4P

A) Superimposition of PilA1 and TcpA from *V. cholerae*. PilA1 is shown in blue, TcpA in grey. B) Pilus fiber model of PilA1 based on the TCP of *V. cholerae*. A predicted salt bridge between Lysine 30 and Glutamate 75 is depicted. C) Superimposition of PilA1 and PilJ; PilA1 is shown in blue, PilJ in chocolate. Side-chains from Lysine 30 and Glutamate 75 (PilA1) / 76 (PilJ) are shown. D) Pilus fiber models showing i) a pilus made up entirely of PilA1, ii) a pilus with PilJ incorporated sporadically and iii) a pilus with PilJ incorporated in clusters.

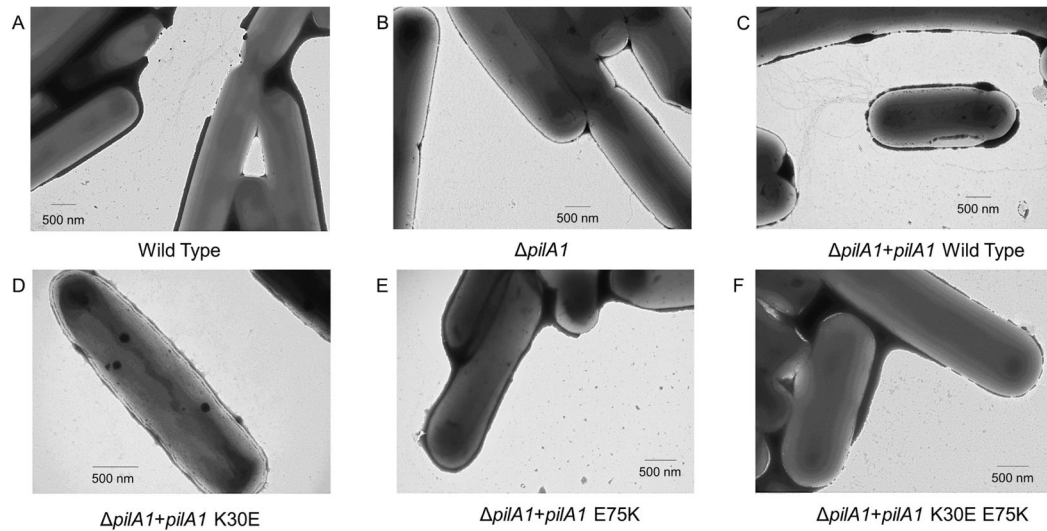


Figure 7. Pilation of PilA1 mutant *C. difficile* Strains

Electron micrographs are shown of A) *C. difficile* R20291 wild type, B) *C. difficile* R20291 with a gene interruption mutant of the *pilA1* gene, *C. difficile pilA1*, C) *pilA1* complemented with *pilA1* wild type, D) *pilA1* complemented with *pilA1* K30E and E) *pilA1* complemented with *pilA1* E75K and F) *pilA1* complemented with *pilA1* K30E E75K.

Table 1

Crystallographic Parameters

Data collection and refinement parameters for MBPPIA1 R20291, NAP08 and CD160 are shown.

| <u>Crystallographic Parameters</u> | <u>MBP-PIA1 R20291</u> | <u>MBP-PIA1 NAP08</u> | <u>MBP-PIA1 CD160</u> |
|------------------------------------|---------------------------------|------------------------------|--------------------------------|
| Resolution range (Å) | 38.58 – 1.899 (1.966 – 1.899) | 59.31 – 2.23 (2.313 – 2.234) | 36.59 – 1.724 (1.785 – 1.724) |
| Space group | C 1 2 1 | P 21 21 21 | I 1 2 1 |
| Unit cell | 143.951 79.366 164.746 90.23 90 | 66.224 74.71 97.517 90 90 90 | 62.484 70.468 117.153 90.24 90 |
| Total reflections | 998770 (98860) | 47582 (4141) | 97145 (5144) |
| Unique reflections | 139534 (14028) | 23808 (2087) | 51185 (784) |
| Multiplicity | 7.1 (7.0) | 2.0 (2.0) | 6.7 (6.6) |
| Completeness (%) | 95.19 (92.48) | 98.73 (87.51) | 95.27 (69.38) |
| Mean I/sigma(I) | 8.74 (1.14) | 14.14 (2.00) | 11.99 (7.25) |
| Wilson B-factor | 22.94 | 26.63 | 27.53 |
| R-merge | 0.1776 (1.844) | 0.04727 (0.4165) | 0.09605 (0.1519) |
| R-meas | 0.1914 | 0.06684 | 0.1043 |
| R-work | 0.1969 (0.2887) | 0.2011 (0.2608) | 0.1968 (0.3684) |
| R-free | 0.2326 (0.3136) | 0.2476 (0.3051) | 0.2218 (0.4014) |
| Ramachandran favored (%) | 98 | 97 | 99 |
| Ramachandran outliers (%) | 0 | 0.4 | 0 |
| Average B-factor | 25.60 | 29.10 | 33.30 |
| Macromolecules | 25.20 | 29.20 | 32.80 |
| Ligands | 29.40 | 16.70 | 27.40 |
| Solvent | 29.20 | 29.10 | 38.60 |